Ultrafast modification of the electronic structure of a correlated insulator

O. Grånäs[1*], I. Vaskivskyi[1,2], P. Thunström[1], S. Ghimire[3], R. Knut[1], J. Söderström[1], L. Kjellsson[1], D. Turenne[1], R. Y. Engel[4], M. Beye[4], J. Lu[3], A. H. Reid[5], W. Schlotter[5], G. Coslovich[5], M. Hoffmann[5], G. Kolesov[6], C. Schüßler-Langeheine[7], A. Styervoyedov[8], N. Tancogne-Dejean[9], M. A. Sentef[9], D. A. Reis[3], A. Rubio[9,10], S. S. P. Parkin[8], O. Karis[1], J. Nordgren[1], J.-E. Rubensson[1], O. Eriksson[1,11], H. A. Dürr[1*]

[1] Department of Physics and Astronomy, Uppsala University, Uppsala, Sweden
[2] Center for Memory and Recording Research, University of California San Diego, 9500 Gilman Drive, La Jolla, CA 92093-0401, USA.
[3] Stanford PULSE Institute, SLAC National Accelerator Laboratory, 2575 Sand Hill Road, Menlo Park, CA 94025
[4] Department of Photon Science, DESY, Notkestraße 85, D-22607 Hamburg, Germany
[5] SLAC National Accelerator Laboratory, 2575 Sand Hill Road, Menlo Park, CA 94025, USA.
[6] John Paulson School of Engineering and Applied Sciences, Harvard University, Cambridge, Massachusetts 02138, USA
[7] Helmholtz-Zentrum Berlin für Materialien und Energie GmbH, 12489 Berlin, Germany
[8] Max-Planck Institut für Mikrostrukturphysik, Weinberg 2, Halle, Germany
[9] Max Planck Institute for the Structure and Dynamics of Matter and Center for Free-Electron Laser Science, Luruper Chaussee 149, 22761 Hamburg, Germany
[10] Center for Computational Quantum Physics, Flatiron Institute, New York, NY 10010 USA
[11] School of Science and Technology, Örebro University, SE-701 82, Örebro, Sweden
[*] e-mail: oscar.granas@physics.uu.se; hermann.durr@physics.uu.se

Electronic materials properties are determined by the interplay of many competing factors. Electro-magnetic fields strong enough to rival atomic interactions can disturb the balance between kinematic effects due to electrons hopping between lattice sites and the Coulomb repulsion between electrons that limits the band formation [1,2]. This allows for new insights into quantum phases, as well as the time-scales and energies involved in using quantum effects for possible applications [3-7]. Here we show that 0.2 V/Å ultrashort optical fields in the high harmonic generation regime [1] lead to a pronounced transient inter-site charge transfer in NiO, a prototypical correlated electron insulator. Element-specific transient x-ray absorption spectroscopy detects a negligible change in electron correlations of Ni 3*d*-states. This behaviour is captured by time-dependent density functional theory and points to a speed limit for the dynamical screening of the Coulomb interaction taking place above our experimental 6.9 femtoseconds optical cycle.

Nickel oxide is a prototype correlated electron material, where signatures of localized atomic-like states [8] as well as band-like dispersive electronic states [9] coexist. The localized states originate from Ni 3*d*-orbitals where the Coulomb repulsion between 3*d*-electrons is only weakly screened. The screened Coulomb interaction, often denoted "Hubbard *U*", gives rise to a band-gap of about 4 eV and is hence a necessary ingredient to be treated on the same footing as the kinetic energy, *t*, of hopping electrons in order to describe the electronic structure of NiO (see Fig. 1 and methods). In the seminal work by Sawatzky and Allen, it was furthermore revealed that the Coulomb repulsion is necessary, but not sufficient, to describe the large energy gap in

NiO [10]. Including dynamic correlations allows an adequate description of the balance between kinematic effects and the Coulomb repulsion [11-13], so that the measured electronic structure of the valence band is reproduced by theory [14]. It was shown [10] that the O 2*p*-states have a fundamental impact on optical and electrical transport properties. These states are often associated with the charge-transfer energy-scale, as their energetic overlap allows electron transfer from O 2*p*-states to the localized Ni 3*d*-states. This mechanism is also relevant for the so-called super-exchange mechanism (of 18 meV strength in NiO) responsible for the antiferromagnetic order between Ni-atoms along the Ni-O-Ni bond direction[15].

Here, we transiently disturb the balance between kinetic energy, t, and the screening of the local Coulomb interaction, U, in NiO by strong external sub-resonant optical fields (i.e. with ~0.6 eV photon energy significantly below the NiO band gap as described in the methods section). The optical field-strength was varied between 0.11 and 0.22 V/Å (see Fig. 3b) corresponding to optical pump fluences of 30 and 120 mJ/cm^2, respectively. In this regime multi-photon transitions as well as Zener tunnelling between valence and conduction states are largely avoided (see methods). The electronic response to external electromagnetic fields of a correlated material is expected to be governed primarily by two effects that may occur simultaneously: a dynamical hopping renormalization [3,16] and a dynamic Hubbard U renormalisation [2] (see methods section). The former is connected to field-induced changes in the electron kinetic energy, modifying the hopping parameter t, while the latter involves large changes in electronic screening and, therefore, a dynamic modification of U. The electronic response of NiO to these scenarios is illustrated in Fig. 1 for O 2*p*- and Ni 3*d*-states of the occupied valence and unoccupied conduction bands.

In the scenario dominated by the dynamical hopping renormalisation, electrons are accelerated along the direction of optical polarization. This results in a transient broadening of the electronic levels via the dynamical Franz-Keldysh effect [3,16], with valence and conduction states leaking into the energy gap region (E_g defined in Fig. 1a). This regime is characterised by the so-called Keldysh parameter (~5 in our case, see methods). In such conditions the electrons adjust non-adiabatically to the external field, hence, remaining in a distorted valence band. Note that for a lower Keldysh parameter values electrons are predominantly promoted from the valence to the conduction band [3]. Thus, the dynamical Franz-Keldysh effect signifies an apparent broadening of the electronic density of states with respect to its ground state [3,16], while for electronic bands that are narrow with respect to the field strength, features of replica bands according to the Wannier-Stark ladder may be visible [17].

The other scenario of dynamical Hubbard U renormalization may occur when strong electron correlations are present. The interaction between localized Ni *3d* and itinerant O 2*p* electrons screens the Hubbard U from an atomic value of 20-25 eV to 7-8 eV [18]. In this scenario, strong electromagnetic fields can influence crystal field levels and ligand states, causing significant changes in screening, i.e. a renormalization of the Hubbard U to a new value $\widetilde{U}$. This is schematically shown in Fig. 1b, where expected changes of the band-gap, as well as the splitting between upper and lower Hubbard bands are illustrated. Recent calculations predict that the local Coulomb repulsion could be modified in NiO by optical fields up to about 0.3 V/Å strength when the photon-energy is significantly below the band-gap [2]. However, the time-scale and the involved screening response remains uncorroborated by experiments. The confirmation of this scenario would allow for new ways of probing ultrafast interactions within a correlated material, and in this way impacting everything from engineering of quantum states to the dielectric breakdown of correlated insulators.

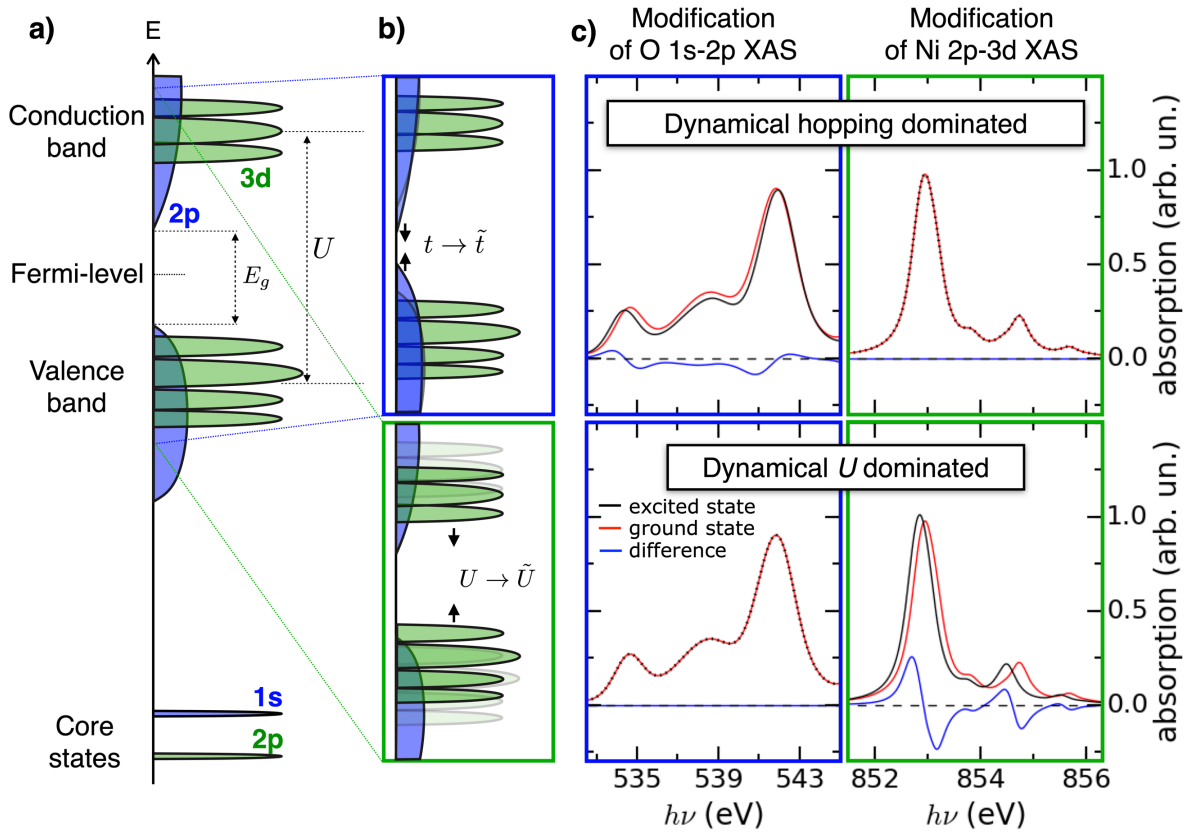

Fig. 1. NiO electronic structure and changes induced by modifying electronic parameters. **a**, Schematic density of electronic states for oxygen (blue) and nickel (green) orbitals. Valence and conduction band oxygen 2p-states, energetically located below and above the Fermi level, show bandlike behaviour and are separated in energy by the band gap, E_g. Valence and conduction band 3*d*-states are split by the Coulomb repulsion between 3*d*-electrons (Hubbard *U*). They display multiplet peaks due to their localized character. **b,** Schematic illustration of expected changes of 2p and 3d-states in the dynamical hopping and dynamical U dominated scenarios discussed in the text. Experimentally these changes are probed via x-ray induced electronic transitions into the respective conduction band states in x-ray absorption spectroscopy (XAS). **c,** Expected changes in the XAS spectra for O 1*s*-2*p* (blue framed picture) and 2*p*-3*d* (green framed picture) transitions modelled by adjusting the band-width ($t \rightarrow \tilde{t}$), and changing screening ($U \rightarrow \tilde{U}$) as described in the methods section. Shown are the spectra in the ground state (red) and for the modified models representing the state driven by strong transient electric fields (black lines), as well as the differences of the two (blue lines). This enables the experimental verification of the two scenarios. While for the dynamical hopping dominated case the oxygen (O) XAS displays pronounced changes, a dynamical *U* dominated effect will predominantly show up in the nickel (Ni) XAS.

We use transient x-ray absorption spectroscopy (XAS) performed at an x-ray free electron laser to distinguish between the two scenarios for NiO (see Fig. 1 and methods). If the dynamical hopping renormalization dominates, we expect a transient change of the O 1*s*-2*p* XAS. If the dynamical *U* renormalization dominates, we expect a respective change of the Ni 2*p*-3*d* XAS. Figures 2a, b show XAS spectra taken in temporal coincidence with the pump optical laser pulses, i.e. at zero pump-probe time-delay of Fig. 2c. It is evident that there is a laser-induced modification of the O 2*p* conduction band (Fig. 2a). However, changes of the Ni 3*d*-states are below the experimental detection limit (Fig. 2b). Before entering the discussion of time dependent phenomena, we note that the spectra from the static situation (red curves, marked "ground state" in Fig. 2a, b, are in good agreement with the calculated spectra in Fig. 1, both for the O 1s-2p and the Ni 2p-3d XAS. This level of agreement has been known, since the works of references [10,19,20].

The changes visible in the O 1*s*-2*p* XAS of Fig. 2a indicate that, when the laser-pump and x-ray-probe pulses arrive simultaneously, a spectral weight transfer takes place in the electric field modified conduction band away from the peaks observed for the ground state. This is clearly visible in the difference spectra (blue line in Fig. 2a) where the XAS peak intensity is

attenuated while spectral weight appears at the wings of the peak both at higher and lower x-ray energies. Such a spectral broadening is reminiscent of the driving field cycle resolved dynamical Franz-Keldysh effect observed with attosecond spectroscopy in semiconductors [16] or Wannier-Stark states in insulators [3]. We note that in our experiments we do not resolve the spectral changes during individual cycles of the laser driving field but rather average over the whole driving pulse.

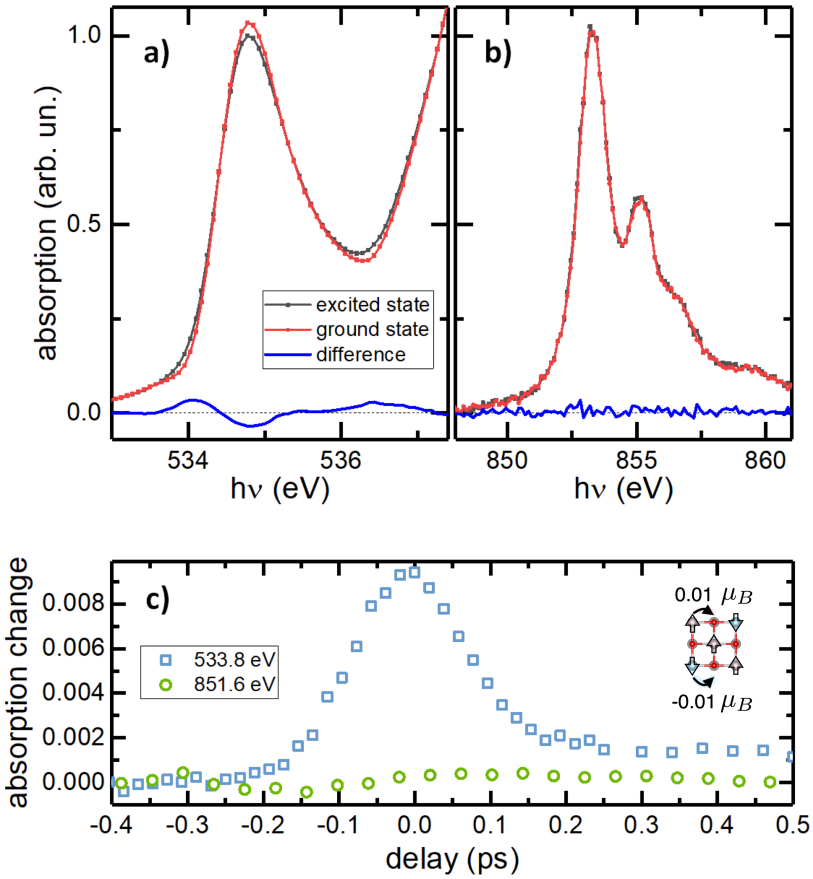

Fig. 2. Experimental transient electronic structure changes seen with XAS.
a, Measured XAS spectra for O 1s-2p transitions and **b**, for Ni 2p-3*d* transitions. Shown are measurements with (black lines) and without (red lines) the driving laser (at 120 mJ/cm^2 fluence), as well as the difference (blue lines) for the laser electric field E||[100] (see Fig. 3). **c**, Temporal evolution of the changes in O (blue squares) and Ni (green circles) XAS vs. pump-probe time-delay. The peak around zero time-delay of the O XAS represents the response shown in **a** and its width is essentially given by the temporal convolution of pump and probe pulses. After ~0.2 ps long-lasting changes to O 2*p* and to a smaller degree also Ni 3*d* orbitals are visible. The O XAS signal has been measured at 533.8 eV x-ray energy while the Ni XAS was obtained for 851.6 eV (see **a** and **b**). The inset shows a schematic view of the transfer of magnetization density from Ni-atoms to O-atoms, indicating the maximum size of the effect. Calculations presented in Fig. 4 indicate a total induced magnetic moment on oxygen atoms of up to 0.01 μ_B

In addition to the XAS measurements, we studied the crystal orientation dependence of high-order harmonics from NiO subjected to driving optical laser fields[1] (see methods). Results are shown in Fig. 3a. We find that the results show maxima along cubic directions, i.e. when the laser field is parallel to the [100] direction. In fact, the signal along [100] is about an order of magnitude higher than that along [110]. This behaviour is consistent with the microscopic mechanism, where a highly preferential charge transfer occurs in the direction where O 2*p* orbitals are well extended and overlapped with Ni 3*d* orbitals [29]. Because the high-harmonic generation process is extremely non-linear such a pronounced affect can be observed and is

even more pronounced with increasing order number as illustrated by the decreasing order width (see Fig. 3a).

Consistent with the angular dependence observed for high harmonic generation we see that the changes in the in O 1s-2p XAS are more pronounced when the pump polarization is along the [100] rather than the [110] direction (see Fig. 3b). This demonstrates that it is the O 2p orbitals that display a pronounced directional polarizability in response to the external electric field. A rationale for this is the chemical bonding of NiO, where a direct overlap of Ni 3*d*- and O 2*p*-states forms Ni-O-Ni bonds in the [100] direction. The [110] direction is rotated by 45°, so that the orbital overlap between Ni 3*d* and O 2*p* states is weaker. A schematic view of the orbital structure is depicted in Fig. 4a, a full Wannier reconstruction of the bands is available in references [19,21].

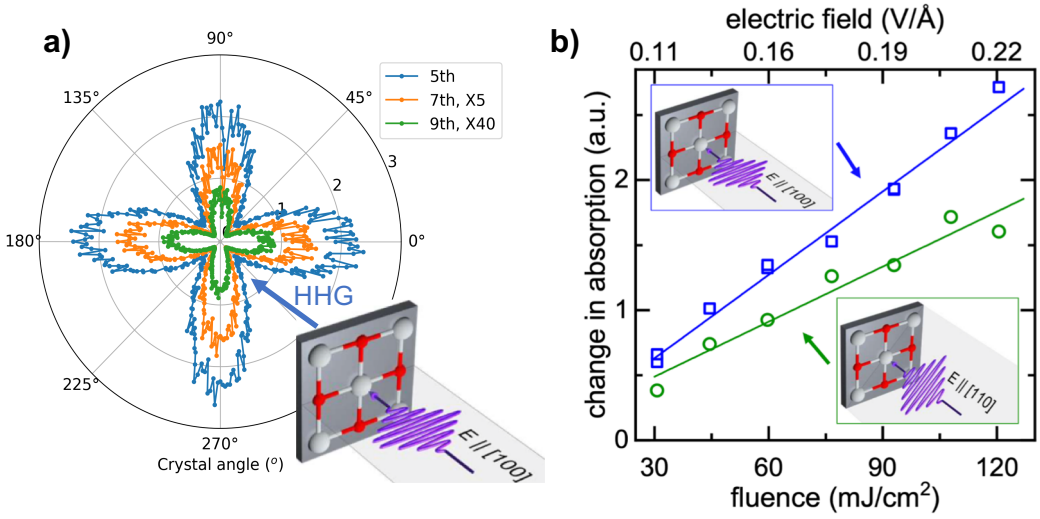

Fig. 3. Crystal orientation dependent electronic structure changes. a, Measurements of the high-harmonic emission of the driving optical laser field vs. crystal angle relative to the [100] direction as schematically shown in the inset. The measured 5th, 7th and 9th harmonics show a strong preference for E || [100] directions. The width of the angular distribution decreases with increasing harmonic order. **b**, Optical pump – XAS probe measurements as in Fig. 2a for two crystal directions as indicated in the insets. Show are the pump-laser fluence (bottom axis) and electric peak field (top axis) dependence of the pumped-unpumped difference in O 1s-2p XAS intensity measured at an x-ray energy of 533.8 eV.

We modelled the dynamical hopping renormalisation response of NiO by solving the time-dependent Schrödinger equation including the external optical field as a vector potential $\vec{E}$, (see methods). The fact that the experimentally measured response of O 2*p*-states dominates over the response of Ni 3*d*-states allowed us to make the simplifying assumption that U is time-independent. Figure 4 displays the results calculated for one half-cycle of a sine wave driving field with duration and amplitude identical to the experimentally applied external field. Initially we focus on changes of the charge density at the Ni and O sites shown in Fig. 4a for two time-steps, $t_1 = \frac{T}{8}$ and $t_2 = \frac{T}{4}$, where T is the cycle period time of 6.9 fs. The NiO charge density response indicates that there is a transient transfer of charge between neighbour atoms according to the direction of the applied electric field. It is also clear that a far larger response can be seen in the vicinity of O atoms compared to Ni, consistent with the experiments. An interpretation of these results can be found in the stronger localization of the Ni 3*d* states, enforced by the strong attractive Coulomb interaction between the positive Ni nucleus and the nearly localised Ni 3*d* electrons. The more delocalized oxygen *2p* states are dominated by the

kinetic energy term, where $\vec{E}$ acts more strongly and results in a larger modification of the electronic structure. This is consistent with a ground-state estimate of a 50% higher polarizability for O than Ni in NiO (see methods).

We now relate the calculated changes in electron density (Fig. 4a) to the measured transient XAS (Figs. 2,3) by calculating the time evolution of the site-resolved electronic density of states (DOS) as detailed in the methods section. Figure 4b shows the O DOS for energies close to the conduction band edge at times corresponding to half a cycle of $\vec{E}$. At the start of the optical cycle (t = 0 fs) the DOS increases as the conduction band edge is approached above an energy of E - $E_F \approx 2.5$ eV. However, as $\vec{E}$ increases with time Fig. 4b shows that additional states appear at significantly lower energy. There are, as an example, states all the way down to 1.5 eV at t = 2.4 fs. This clearly illustrates the band-widening expected from the dynamical Franz-Keldysh effect [16]. In addition, Fig. 4b demonstrates that the appearance of states within the band-gap lags behind the electric driving field. While $\vec{E}$ reaches its maximum value at t = 1.7 fs, the in-gap states are most pronounced around 2.4 fs. This 0.7 fs delay can be attributed to the contribution of dielectric polarization currents which counteract $\vec{E}$ [3,4,22].

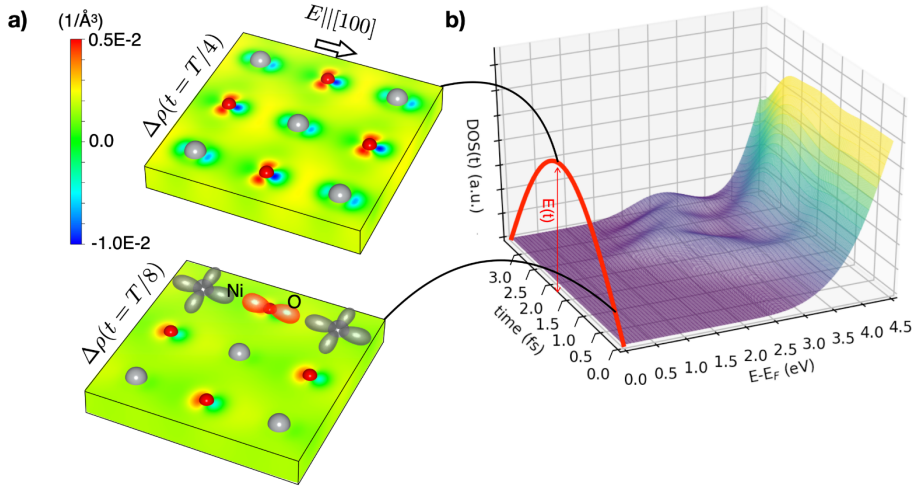

Fig. 4. Calculated transient electronic structure of NiO. a, Calculated charge-density difference, $\Delta\rho$, in real-space as a function of time. The colour represents the difference between the time-dependent and ground-state electron density, with the scale according to the colour-bar. Red indicates an increase in electron density, and blue a decrease. **b**, Calculated change in single-particle energy expectation value close to the conduction band edge, when driven with one full cycle of the pump-pulse, as indicated by the electric field, E(t), shown as red line. The colour of the electronic density of states (DOS) serves as a guide to the eye and illustrates the number of states per unit energy also shown as the vertical axis. See methods for additional details regarding the calculations.

Our joint experimental and theoretical results demonstrate that the response of NiO to strong sub-resonant electromagnetic fields is predominantly due to transient modifications to the hopping parameter consistent with a transient directional charge transfer from O to Ni. This is observed both as a dynamical Franz-Keldysh effect in the O1*s*-2*p* XAS and a strong directional anisotropy in high harmonic generation experiments, favouring conditions when the pump is polarized along the Ni-O-Ni bonding direction. In addition, we detect no discernible change in the dynamical screening of the Coulomb interaction. Thus, the optical driving field has for NiO the largest impact on dispersive, delocalised states. Apparently, the screening of the localised Ni *3d states* is too slow to follow the modulation of the more dispersive states enacted by the optical field under the present experimental conditions. From our measurements of the electronic structure at times after the driving field has been switched off, we find an intriguing persistent modification of the NiO band-gap (see Fig. 2c). This finding has significant

implications for future experimental and theoretical developments, and potentially for technological applications.

Since the Ni-O-Ni bond is responsible for mediating the super-exchange interaction that governs the equilibrium antiferromagnetic order in NiO [23-25], any transient modification of the magnetization-density around the oxygen atom, as implied by the inset of Fig. 2c, must change this magnetic interaction in the resulting non-equilibrium state. Equivalent modifications of the magnetic exchange by sub-gap excitation have been observed using all-optical pump-probe methods [26]. Here we provide the x-ray analogue that clearly demonstrates how the electronic structure is modified by a directional transient charge transfer between O and Ni. Future measurements will be able to probe what type of possible magnetic excitation evolve on ultrafast timescales [27]. The theoretical approach described here has potential to lead the way to guide and interpret such measurements.

Methods

Experimental methods

X-ray Absorption Spectroscopy (XAS) measurements on NiO.

The XAS spectra were measured at the SXR instrument of the Linac Coherent Light Source (LCLS) at SLAC National Accelerator Laboratory in Stanford/USA. The X-ray pulses with linear horizontal polarization were focused by a pair of Kirkpatrick-Baez mirrors and impinged on the sample at 70° with respect to surface resulting in an elliptical beam footprint of 400x80 μm^2. The pulse energy for 50 fs x-ray pulses was set to about 0.3 uJ and 2 uJ at oxygen and nickel edge respectively. This results in values of the x-ray fluence of 0.1 – 0.15 mJ/cm^2 (O 1*s*-2*p* resonance) and 0.65-0.85 mJ/cm^2 (Ni 2*p*-3*d* resonance) on the sample. The spectra were recorded in the x-ray energy ranges of 533-538 eV and 849-861 eV for O 1s-2p and Ni 2p-3d core-valence resonances, respectively. XAS was detected in fluorescence yield mode with large area microchannel plates insensitive to the pump laser photons. The pump laser with the central wavelength of 2 μm (~0.6 eV photon energy) and linear horizontal polarisation from a synchronized femtosecond laser source was coupled collinearly to the x-ray beam. To ensure homogenous excitation of the probed spot the pump spot size was set to ~1 mm. Time-delay traces (Fig. 3) were measured at two fixed photon energies in the pre-edge regions of O and Ni absorption bands. The rise-time of the signal in Fig. 3, as well as overall time-resolution in the experiment was mainly limited by the duration of the pump pulse (~190 fs). To measure the spectra for the two different pump polarizations (E || [100] and E || [110] in Fig. 2b) the sample was rotated by 45°, while keeping the polarization of the pump and probe beams unchanged. This ensured unchanged pump-probe overlap and spot size in both experiments and minimizes the differences due to optical reflections of the pump pulse from the sample. At the highest used pump fluence, permanent damage of the sample occurred after 2-5 min exposure. To avoid degradation of spectra, the sample was moved to a fresh spot every 90 s. The characteristics of the pump and probe pulses are determined so as the combined intensity is below the damage threshold of the sample. All measurements shown here were performed at room temperature, i.e. below the equilibrium NiO antiferromagnetic ordering Neel temperature of 525 K, which is determined largely by an exchange coupling of 18 meV [28].

Optical High-harmonics generation (HHG) in NiO.

High-order harmonics were measured in the transmission geometry at normal incidence, independently to the XAS measurements but in similar laser conditions. The light source was an optical parametric amplifier (OPA, HE-TOPAS-Prime, Light Conversion) pumped by a Ti:sapphire amplifier system (Legend Elite Duo, Coherent) operating at a 1 kHz repetition rate. The idler pulse at ~2.08 μm in wavelength from the OPA was loosely focused onto the NiO

side of the sample. The pulse duration is around 60 fs. The area of the focal spot on the sample surface was estimated to be ~0.0297 cm^2 from a knife edge measurement. The pulse energy was set at 16 μJ. The high-harmonic beam propagating along the transmission direction was collected by a lens and focused into the entrance slit of a spectrometer, which consisted of a grating-based monochromator (Acton, VM-504, grating: 300 grooves mm^{-1}) and a charge-coupled device (CCD, Andor DO440). Spectrally resolved high-harmonic signals emerging from the NiO film were recorded by the CCD. A bare MgO substrate was tested under the same laser fluence and only third-harmonic signal was observed [29]. This confirms that the reported HHG signals all emerged from the NiO film. Because of the wider band-gap in MgO, it requires a higher fluence to produce high-harmonics that are detectable. Similarly, reported harmonics have photon energy below the bandgap of MgO substrate and therefore the substrate is transparent.

Sample growth.
The NiO layers used in the experiments were grown on double polished MgO(001) substrates. Polishing both front and back sides of the MgO substrate ensured that the XAS samples could also be used for HHG experiments. A 2 nm thick MgO underlayer was deposited by RF magnetron sputtering in 3 mTorr argon at a temperature below 100 C followed by a NiO layer that was deposited at 700 C in an Ar(90%)/O_2(10%) gas mixture at a pressure of 3 mTorr and was then annealed in-situ at the same temperature (700 C) for 15 min in the same Ar-O_2 gas mixture. In addition, 30 nm thin NiO transmission films were used for tuning the x-ray energy when setting up the experiment. They were grown by molecular beam epitaxy on 200 nm Si_3N_4 membranes. Ni metal was evaporated in an oxygen atmosphere of $3 \cdot 10^{-7}$ mbar, the substrate was held at 250 C, the growth rate was 1.8 Å/min.

Computational methods
Determining optimal pump characteristics
In order to minimise the number of electrons that the pump-pulse excites to the conduction band, we tailor our pump pulse to minimize Zener-tunnelling and multi-photon transitions, and of course direct transitions. To achieve this goal, we use the so-called Keldysh-parameter, γ_k, relating materials- and pulse-properties to estimate the regime we are operating in. The dynamical Franz-Keldysh effect has previously been studied in wide band-gap semiconductors, with $\gamma_k \approx 3$ [16]. Studies exploring conditions for Zener-tunnelling are also available, indicating a lower bound in the range of $\gamma_k \approx 3$. We ensure our pulse is slightly above this lower bound. Additionally, we need to keep the combined pump- and probe-pulse intensity below the damage threshold, while still allowing us to probe both the O 1*s*-2*p* and Ni 2*p*-3*d* resonances. The optical gap of NiO at room temperature is reported to be 3.4 eV-4.0eV, the reduced effective carrier mass of NiO is $m \sim 1 m_e$. With the conditions for γ_k in mind we experimentally use a maximum field amplitude and photon energy of E_0 =0.22 V/Å and ω_0 =0.6 eV, respectively. leading to $\gamma_k \approx 5$, a suitable range of ponderomotive energy in relation to materials characteristics [30,31].

First-principles calculations
Conventional first principles methods based on Kohn-Sham density-functional theory in the semi-local approximation, e.g. GGA [32] fails to reproduce many of the features of strongly correlated electron materials. Nickel oxide shows signatures of localized atomic-like states as well as band-like electronic states with significant dispersion. To account for the weakly screened Coulomb repulsion between electrons of *d*-character, an on-site term adopted from the Hubbard Hamiltonian, often denoted "Hubbard *U*", is included in the Hamiltonian. A *U*-value of 7-8 eV results in an appropriate band-gap of about 4 eV, which is an order of magnitude

larger than that predicted by pure semi-local DFT. Our calculations aim to reproduce the behaviour of NiO below the Néel temperature, and is thus anti-ferromagnetically ordered [33].

To support our experimental data and to interpret our results, we use different flavours of the DFT+U Hamiltonian to describe the system, according to the sub-sections below.

X-ray absorption spectroscopy calculations for NiO

The XAS spectra of the Ni L-edge in Figure 1 are obtained from a multi-configurational approach based on density-functional theory combined with multiplet ligand field theory [19,20] for the Ni 3d states, using the parameters from Ref. [20]. The presence of the core-hole of the 2p shell and its non-trivial coupling to the valence electrons is explicitly included in the calculations, as implemented in a full-potential, linear muffin-tin orbitals method (RSPt) [34]. Figure 1c shows a qualitative estimate of how the XAS spectra are modified in the presence of a strong dynamical screening of U ($U \rightarrow \widetilde{U}$). This was modelled by reducing the effective U from 6.9 eV to 6.2 eV, which also modifies the double counting correction from 100.2 eV to 94.6 eV. To estimate the effect of a modulated hopping term ($t \rightarrow \tilde{t}$) on the XAS of the O 1*s*-2*p* transitions, we performed calculations of NiO in the AFM ordered phase using the APW+lo software Elk [35]. The band-broadening was induced by compressing the lattice 1% from the equilibrium geometry. Further, the maximum number of plane-waves to include in the basis was determined by setting the maximum $|\boldsymbol{G} + \boldsymbol{k}| \cdot R_{MT}$ to 8, where R_{MT} is the average radius of the augmentation muffin tins, $\boldsymbol{G}$ is a reciprocal lattice vector, and $\boldsymbol{k}$ a crystal momentum within the first Brillouin zone. The full Brillouin-zone was sampled by 12^3 *k*-points in order to perform integrations. Similar settings where used to calculate the band-structure and band-character of NiO. The muffin-tin radius was varied in order to estimate the gradient of oxygen to nickel character on the interstitial states.

Polarizability

The polarizabilities α of Ni and O where estimated in GGA+U using the VASP software [36,37]. Here, the atomic polarizabilities are scaled according to how the atomic charge is rearranged in the solid according to an iterative scheme based on Hirshfeld partitioning of the self-consistent charge-density [38,39].

Time-dependent density response and density of states

The implementation of time-dependent density-functional theory used to determine the transient changes in charge density and density of state, as shown in figure 3, is based on an extension of the Siesta software [40], as described in Kolesov *et al*. [41]. Further, the vector potential and coupling to macroscopic fields are implemented according to Bertsch et al [42]. The external field is included in the Coulomb-gauge, as a vector potential of $A(t) = -\overrightarrow{E_0}\int_{t_0}^{t} \sin(\omega t')\, dt'$, where $\overrightarrow{E_0} = 0.2$ V/Å in the [100] direction, $T = 6.9$ fs and $\omega = 0.6\ eV$. The basis set consists of numerical atom-centred double-Zeta + polarization orbitals. Grid integrals are performed on an equidistant mesh with a 120 Ry cut-off. The real-time propagation is performed in time-steps of 6.05 atto-seconds. The local magnetic moment and charge transfer is extracted from Mulliken charges associates with the atom-centred orbitals. Indicating that the majority of charge transfer is associated with O $2p_x$ and Ni *4s* states. The time-evolved density of states is calculated as the sum of expectation values of the time-evolved wave-functions, i.e. $\epsilon_i(t) = \langle \phi_i(t)|H(t)|\phi_i(t)\rangle$, represented with a gaussian broadening of 0.3 eV. The exchange and correlation were treated within the generalized gradient + Hubbard U approximation (GGA+U) [32,43]. The effective U is set to 7 eV, reproducing the experimental band-gap of 4 eV. In our calculation we keep the effective U fixed. When allowing for a dynamical response of U as an

adiabatic functional of the density matrix (no retardation/memory effects in the functional), one sees pronounced changes of U and thus the electronic structure involving also bands of primarily Ni 3*d*-character. This is contrary to the experimental findings under the pump-characteristics we have considered here. This points in turn to the importance of developing the theory for real-time dynamics of strongly correlated materials further, beyond the adiabatic treatment of screening for first principles non-equilibrium dynamics [44].

Visualizations are made in Vesta [45], and using python/matplotlib [46].

Acknowledgement
OG acknowledges the Swedish National Infrastructure for Computing (SNIC) for the allocation of computing time at NSC and HPC2N. OG acknowledge financial support from the Strategic Research Council (SSF) grant ICA16-0037 and the Swedish Research Council (VR) grant 2019-03901. O.E. acknowledges support from the Swedish Research Council (VR), the Knut and Alice Wallenberg (KAW) foundation, the Foundation for Strategic Research (SSF), the European Research Council (ERC), and eSSENCE. HAD acknowledges support from the Swedish Research Council (VR) grants 2017-06711and 2018-04918. MB and RYE are funded by the Helmholtz Association through grant VH-NG-1105. IV acknowledges support by the U.S. Department of Energy, Office of Science, Office of Basic Energy Sciences under the X-Ray Scattering Program Award Number DE-SC0017643. Operation of LCLS is supported by the U.S. Department of Energy, Office of Basic Energy Sciences under contract No. DE-AC02-76SF00515. Work at Pulse was supported by the AMOS program within the Chemical Sciences Division of the Office of Basic Energy Sciences, Office of Science, U.S. Department of Energy. SG, JL and DAR acknowledge the support and SG additionally acknowledges the Early Career Research Program. Work at CFEL was supported by the European Research Council (ERC-2015-AdG-694097), Grupos Consolidados (IT1249-19) and the Flatiron Institute, a division of the Simons Foundation. We acknowledge funding by the Deutsche Forschungsgemeinschaft (DFG) under Germany's Excellence Strategy - Cluster of Excellence Advanced Imaging of Matter (AIM) EXC 2056 - 390715994 and funding by the Deutsche Forschungsgemeinschaft (DFG). MAS acknowledges funding through the Emmy Noether Programme of Deutsche Forschungsgemeinschaft (SE 2558/2-1).

Author contributions
HAD conceived the experiment in discussions with NGT, MS, AR and DAR. OG, PT, GK, and OE performed the computational study. OG, GK, NGT, MS and AR developed the underlying methodology for the time-dependent DFT calculations. IV, RSG, RK, JS LK, DT, RYE, MB, JL, GK, CSL, AHR, WS, GC, MH, AS, SSPP, OK, JN, JER, HAD performed the experiments and analysed the results. All authors contributed to the manuscript.

Competing Interests
The authors declare no competing financial interests

Correspondence and requests for materials should be addressed to OG or HAD.

References
1. Ghimire, S. & Reis, D. A. High-harmonic generation from solids. *Nature Physics* 1–7 (2018). doi:10.1038/s41567-018-0315-5
2. Tancogne-Dejean, N., Sentef, M. A. & Rubio, A. Ultrafast Modification of Hubbard U in a Strongly Correlated Material: Ab initio High-Harmonic Generation in NiO. *Phys Rev Lett* **121,** 097402 (2018).

3. Schiffrin, A. *et al.* Optical-field-induced current in dielectrics. *Nature* **493,** 1–7 (2012).
4. Schultze, M. *et al.* Controlling dielectrics with the electric field of light. *Nature* **493,** 75–78 (2012).
5. Popmintchev, D. *et al.* Near- and Extended-Edge X-Ray-Absorption Fine-Structure Spectroscopy Using Ultrafast Coherent High-Order Harmonic Supercontinua. *Phys Rev Lett* **120,** 093002 (2018).
6. Stojchevska, L. *et al.* Ultrafast switching to a stable hidden quantum state in an electronic crystal. *Science* **344,** 177–180 (2014).
7. Gray, A. X. *et al.* Ultrafast terahertz field control of electronic and structural interactions in vanadium dioxide. *Phys Rev B* **98,** 045104 (2018).
8. Groot, F. de. Multiplet effects in X-ray spectroscopy. *Coordination Chemistry Reviews* **249,** 31–63 (2005).
9. Shen, Z. *et al.* Electronic structure of NiO: Correlation and band effects. *Phys Rev B* **44,** 3604–3626 (1991).
10. Sawatzky, G. A. & Allen, J. W. Magnitude and Origin of the Band Gap in NiO. **53,** 2339–2342 (1984).
11. Metzner, W. & Vollhardt, D. Correlated Lattice Fermions in d=inf Dimensions. **62,** 324–327 (1989).
12. Georges, A., Kotliar, G., Krauth, W. & Rozenberg, M. Dynamical mean-field theory of strongly correlated fermion systems and the limit of infinite dimensions. *Rev Mod Phys* **68,** 13–125 (1996).
13. Kotliar, G. *et al.* Electronic structure calculations with dynamical mean-field theory. *Rev Mod Phys* **78,** 865–951 (2006).
14. Thunstrom, P., Di Marco, I. & Eriksson, O. Electronic Entanglement in Late Transition Metal Oxides. *Phys Rev Lett* **109,** 186401–5 (2012).
15. Betto, D. *et al.* Three-dimensional dispersion of spin waves measured in NiO by resonant inelastic x-ray scattering. *Phys Rev B* **96,** 020409–5 (2017).
16. Lucchini, M. *et al.* Attosecond dynamical Franz-Keldysh effect in polycrystalline diamond. *Science* **353,** 916–919 (2016).
17. Wannier, G. Wave Functions and Effective Hamiltonian for Bloch Electrons in an Electric Field. *Physical Review* (1960).
18. Panda, S. K., Jiang, H. & Biermann, S. Pressure dependence of dynamically screened Coulomb interactions in NiO: Effective Hubbard, Hund, intershell, and intersite components. *Phys Rev B* **96,** 045137–14 (2017).
19. Haverkort, M. W., Zwierzycki, M. & Andersen, O. K. Multiplet ligand-field theory using Wannier orbitals. *Phys Rev B* **85,** 165113–20 (2012).
20. Lüder, J. *et al.* Theory of L -edge spectroscopy of strongly correlated systems. *Physical Review B (accepted)* **96,** 245131 (2017).
21. Wu, M. *et al.* Strain and composition dependence of orbital polarization in nickel oxide superlattices. *Phys Rev B* **88,** 125124–9 (2013).
22. Kruchinin, S. Y., Krausz, F. & Yakovlev, V. S. Colloquium: Strong-field phenomena in periodic systems. *Rev Mod Phys* **90,** 021002 (2018).
23. Kramers, H. A. L'interaction Entre les Atomes Magnétogènes dans un Cristal Paramagnétique. *Physica* **1,** 182–192 (1934).
24. Anderson, P. W. Antiferromagnetism. Theory of Superexchange Interaction. *Physical Review* (1950).
25. Goodenough, J. B. Theory of the Role of Covalence in the Perovskite-Type Manganites. *Physical Review* **100,** 564–573 (1955).
26. Kirilyuk, A., Kimel, A. V. & Rasing, T. Ultrafast optical manipulation of magnetic order. *Rev Mod Phys* **82,** 2731–2784 (2010).

27. Iacocca, E. *et al.* Spin-current-mediated rapid magnon localisation and coalescence after ultrafast optical pumping of ferrimagnetic alloys. *Nat Commun* 1–11 (2019). doi:10.1038/s41467-019-09577-0
28. Hutchings, M. T. & Samuelsen, E. J. Measurement of spin-wave dispersion in NiO by inelastic neutron scattering and its relation to magnetic properties. *Physical Review B (accepted)* **6,** 3447–3461 (1972).
29. You, Y. S., Reis, D. A. & Ghimire, S. Anisotropic high-harmonic generation in bulk crystals. *Nature Physics* **13,** 345–349 (2016).
30. Ghimire, S. *et al.* Redshift in the Optical Absorption of ZnO Single Crystals in the Presence of an Intense Midinfrared Laser Field. *Phys Rev Lett* **107,** 1307–5 (2011).
31. Kruchinin, S. Y., Krausz, F. & Yakovlev, V. S. Colloquium: Strong-field phenomena in periodic systems. *Rev Mod Phys* **90,** 021002 (2018).
32. Perdew, J. P. Generalized gradient approximation made simple. *Phys Rev Lett* **77,** 3865–3868 (1996).
33. Roth, W. L. Magnetic structures of MnO, FeO, CoO, and NiO. *Physical Review* **110,** 1333–1341 (1958).
34. Wills, J. M. *et al. Full-Potential Electronic Structure Method, Energy and Force Calculations with Density Functional and Dynamical Mean Field Theory*. **167,** 1–195 (Springer Berlin Heidelberg, 2010).
35. Dewhurst, J. K. *et al. The Elk Code Manual*. 1–184 (2020).
36. Kresse, G. & Furthmuller, J. Efficient iterative schemes for ab initio total-energy calculations using a plane-wave basis set. *Phys Rev B* **54,** 11169–11186 (1996).
37. Kresse, G. & Joubert, D. From ultrasoft pseudopotentials to the projector augmented-wave method. *Phys Rev B* **59,** 1758–1775 (1999).
38. Tkatchenko, A. & Scheffler, M. Accurate Molecular Van Der Waals Interactions from Ground-State Electron Density and Free-Atom Reference Data. **102,** 073005 (2009).
39. Bučko, T., Lebègue, S., Ángyán, J. G. & Hafner, J. Extending the applicability of the Tkatchenko-Scheffler dispersion correction via iterative Hirshfeld partitioning. *J. Chem. Phys.* **141,** 034114 (2014).
40. Soler, J. M. *et al.* The SIESTA method for ab initio order-N materials simulation. *J. Phys. Condens. Matter* **14,** 2745–2779 (2002).
41. Kolesov, G., Grånäs, O., Hoyt, R., Vinichenko, D. & Kaxiras, E. Real-Time TD-DFT with Classical Ion Dynamics: Methodology and Applications. *J Chem Theory Comput* **12,** 466–476 (2016).
42. Bertsch, G. F., Iwata, J. I., Rubio, A. & Yabana, K. Real-space, real-time method for the dielectric function. *Phys Rev B* **62,** 7998–8002 (2000).
43. Dudarev, S. L., Botton, G., Savrasov, S. Y., Humphreys, C. & Sutton, A. Electron-energy-loss spectra and the structural stability of nickel oxide: An LSDA+U study. *Phys Rev B* **57,** 1505–1509 (1998).
44. Tancogne-Dejean, N., Sentef, M. A. & Rubio, A. Ultrafast Transient Absorption Spectroscopy of the Charge-Transfer Insulator NiO: Beyond the Dynamical Franz-Keldysh Effect. *Physical Review B (accepted)*
45. Momma, K. & Izumi, F. VESTA: a three-dimensional visualization system for electronic and structural analysis. *J Appl Crystallogr* **41,** 653–658 (2008).
46. Hunter, J. D. Matplotlib: A 2D Graphics Environment. *Comput Sci Eng* **9,** 90–95 (2007).